THE JOURNAL OF PHYSICAL CHEMISTRY C

Article

pubs.acs.org/JPCC

Odd−Even Effect in the Polymorphism of Self-Assembled Monolayers of Biphenyl-Substituted Alkaneselenolates on Au(111)

Maciej Dendzik,[†] Andreas Terfort,[‡] and Piotr Cyganik*[,†]

[†]Centre for Nanometer-Scale Science and Advanced Materials (NANOSAM), Smoluchowski Institute of Physics, Jagiellonian University, Reymonta 4, 30-059 Kraków, Poland

[‡]Institute of Inorganic and Analytical Chemistry, Goethe University, Max-von-Laue Strasse 7, 60438 Frankfurt, Germany

ABSTRACT: Self-assembled monolayers (SAMs) of ω-(4′-methylbiphenyl-4-yl) alkaneselenolates $CH_3(C_6H_4)_2(CH_2)_nSe^-$ (BPnSe, n = 2−6) on Au(111) substrates, prepared in solution at elevated temperature (333 K), were studied using scanning tunneling microscopy (STM). Molecularly resolved images reveal that even-numbered BPnSe SAMs form two or three different coexisting phases, including the one observed at room temperature. In contrast, odd-numbered species exhibit only a single phase, which is the same as the one observed at room temperature, i.e. close to a commensurate oblique $(2\sqrt{3}\times\sqrt{3})R30°$ structure with two molecules per unit cell. Importantly, one of the phases observed for even-numbered BPnSe/Au(111) at room temperature (α-phase) has a well-defined periodicity only in 1D, whereas the new additional phases observed at elevated temperature are fundamentally different and have 2D periodic character, exhibiting a commensurate rectangular $5\times2\sqrt{3}$ lattice with four molecules per unit cell (β-phase) and an incommensurate oblique $2\sqrt{3}\times1.2\sqrt{3}$ lattice with two molecules per unit cell (γ-phase). For all systems, partial reorientation of the Au(111) step edges was observed upon SAM formation, indicating significant mobility of the topmost gold atoms induced by the adsorbates. To elucidate the effect of the S → Se substitution on the SAMs structure on Au(111), present results for BPnSe/Au(111) systems are discussed in view of the previously reported microscopic, spectroscopic, and desorption data obtained for these SAMs and for their thiol analogs, i.e. for BPnS/Au(111).

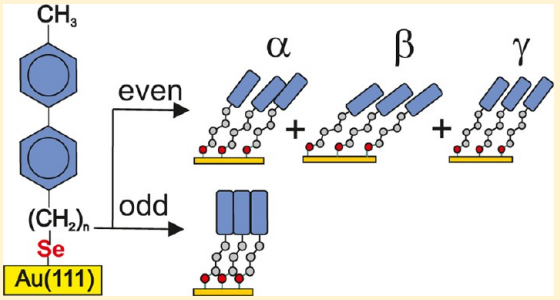

I. INTRODUCTION

The broad range of applications of self-assembled monolayers (SAMs) on Au(111) in nanotechnology qualifies them as a prototype system for surface design.[1] Despite the huge popularity of SAMs on Au(111), which is mainly driven by the ease of formation and modification, their detailed structure remains controversial due to the complicated interplay of molecule−molecule and molecule−substrate interactions in these systems.[2,3] Considering the present difficulties in calculating the structures for even the simplest SAMs on Au(111),[2,3] the rational design of technologically attractive, and thus more complicated, SAMs relies on systematic experimental approaches.

Following this general argumentation and the potential application of aromatic SAMs in molecular electronics,[4,5] systematic studies on the homologous series of the aromatic/aliphatic hybrid system $CH_3-(C_6H_4)_2-(CH_2)_n-S$/Au(111) (BPnS, n = 1−6) have been undertaken.[6−10] For purely aromatic thiolate SAMs on Au(111), the defect density is high, due to the relaxation of stress resulting from the misfit between the lattice preferred by the aromatic moieties and the one of the Au(111) substrate.[11,12] Our study demonstrated that introduction of the aliphatic chain in BPnS/Au(111) can solve this stress problem, since insertion of a flexible aliphatic chain gives additional degrees of freedom, providing other pathways to reduce stress without breaking up the structure preferred by the aromatic moieties.[13] However, insertion of an aliphatic chain, the length of which is described by the parameter n, has deeper consequences for the BPnS/Au(111) SAMs. As demonstrated by previous detailed microscopic[9,10] and spectroscopic[7,8] measurements, the structure of the BPnS/Au(111) SAMs depends strictly on the parity of this parameter and results in a higher density of more upright oriented molecules for the odd-numbered members of this series. This odd−even structural effect influences also the stability of these SAMs toward electrochemical desorption,[14,15] ion-induced desorption,[16] exchange by other thiols,[17,18] and electron irradiation.[19] In all these odd−even effects, related to different aspects of film stability, the odd-numbered BPnS/Au(111) SAMs turn out to be the more stable ones.

In parallel, as another route toward optimization of the quality of aromatic SAMs, we have proposed substitution of the anchoring atom which binds molecules to the Au(111) substrate. Experiments performed for BP0Se/Au(111) demonstrated that substitution of the anchoring S atom by Se permits the formation of SAMs of high structural quality.[20] This observation was also reproduced later by investigations of anthraceneselenolate[21] and anthracenethiolate[12] SAMs on

Received: May 29, 2012
Revised: August 13, 2012

   dx.doi.org/10.1021/jp3051998 | J. Phys. Chem. C XXXX, XXX, XXX−XXX

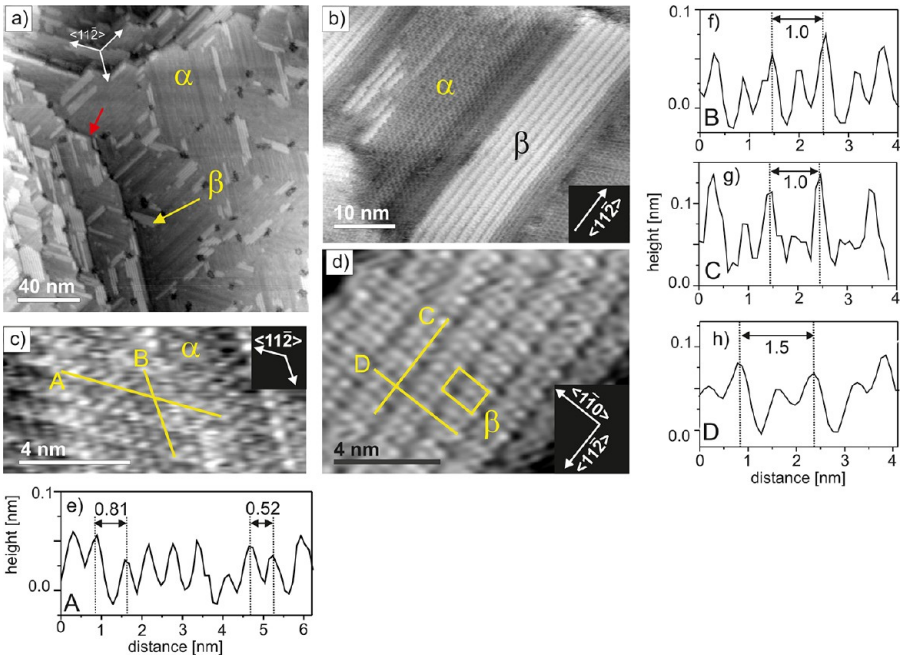

Figure 1. STM data for BP2Se SAMs on Au(111) prepared in 0.1 mM ethanolic solution at 333 K. (a–d) STM images taken with different resolutions. In parts e and f, heights profiles A and B are taken along the lines depicted in part c. In parts g and h, height profiles C and D are taken along the lines depicted in part d. In part a, the red arrow indicates kinks at step edges. In parts a–d, the α and β symbols mark different phases (see text for details). In part d, the rectangular box marks the rectangular $5 \times 2\sqrt{3}$ unit cell of the β-phase with dimensions marked in the height profiles presented in parts g and h, respectively.

Au(111). To understand the impact of this substitution on SAMs structure, we have performed systematic microscopic[22] and spectroscopic[23,24] studies of the selenol analogs of BPnS/Au(111) SAMs vs the $CH_3-(C_6H_4)_2-(CH_2)_n$-Se/Au(111) (BPnSe, n = 1–6) series. These experiments demonstrated that BPnSe/Au(111) SAMs exhibit very similar odd–even structural effects as observed for their thiolate analogs. As a next step to investigate the influence of the S → Se substitution on SAM stability, we have performed recently exchange[18] and ion-desorption experiments[16,25] which demonstrated the odd–even effect in Se–Au and S–Au bond stability as well as higher stability of the Se–Au bond as compared to the S–Au in BPnSe/Au(111) and BPnS/Au(111) SAMs, respectively.

To further elucidate the impact of the S → Se substitution on SAMs structure and stability, in the present experiments, we investigate the influence of the formation temperature on the structure of BPnSe/Au(111) SAMs and compare the results with the corresponding data obtained by us earlier for their thiol analogs.

II. EXPERIMENTAL SECTION

The precursor molecules for BPnSe SAM fabrication were diselenide compounds (BPnSe–SeBPn: $CH_3(C_6H_4)_2(CH_2)_n$Se–Se$(CH_2)_n(C_6H_4)_2CH_3$). The synthesis of these molecules has been described elsewhere.[26] The gold films were prepared at a base pressure of $\sim 10^{-7}$ mbar by evaporating (rate 2 nm/s) 150 nm of gold onto mica substrates at 610 K. Before deposition, the freshly cleaved mica sheets had been heated at the evaporation temperature for about 24 h under vacuum conditions to remove residual water. After deposition, the gold/mica substrates were flame-annealed in a butane/oxygen flame. This procedure yielded high-quality Au-films with flat terraces of several 100 nm exhibiting a (111) surface orientation and steps faceting along the $\langle 1\bar{1}0 \rangle$ directions. The BPnSe SAMs have been prepared by immersion of Au(111) substrates into a 0.1 mM solution of the respective BPn diselenide (BPnSe–SeBPn) in ethanol at 333 K for 24 h. The incubation temperature was selected to be well below the boiling point of ethanol (352 K). This is the same temperature as in our previous studies[9,10] with the thiol analogs (BPnS), making a comparison of the behavior of both types of SAMs possible. After immersion, samples were rinsed with pure ethanol and blown dry with nitrogen.

All STM measurements were carried out in air at room temperature using a MultiMode IIIa Digital Instruments microscope. In all cases, tips were prepared mechanically by cutting a 0.25 mm Pt/Ir alloy (8:2, Goodfellow) wire. The data were collected in constant current mode using tunnelling currents in the range of 20–50 pA and a sample bias between 0.7 and 1.2 V (tip positive). No tip-induced changes were observed under these imaging conditions.

III. RESULTS

The STM data obtained in this study are summarized in Figures 1–4 for even-numbered BPnSe/Au(111) SAMs and in Figures 5 and 6 for odd-numbered BPnSe/Au(111) SAMs. All analyzed samples were prepared by 24 h incubation in ethanolic solution (0.1 mM) of the respective molecules at an elevated temperature of 333 K. The STM analysis was performed in air at room temperature.

Even BPnSe/Au(111) SAMs (n = 2, 4, 6). Results obtained for the BP2Se/Au(111) system are presented in Figure 1. Data obtained at large scale are shown in Figure 1a and reveal two interesting features, i.e. characteristic kinks at step edges (indicated by red arrow) and sample areas showing clearly different contrast labeled by α and β letters. These areas labeled by α and β correspond to two different molecular structures, as is more clearly visible in Figure 1b. High resolution data are

dx.doi.org/10.1021/jp3051998 | J. Phys. Chem. C XXXX, XXX, XXX–XXX

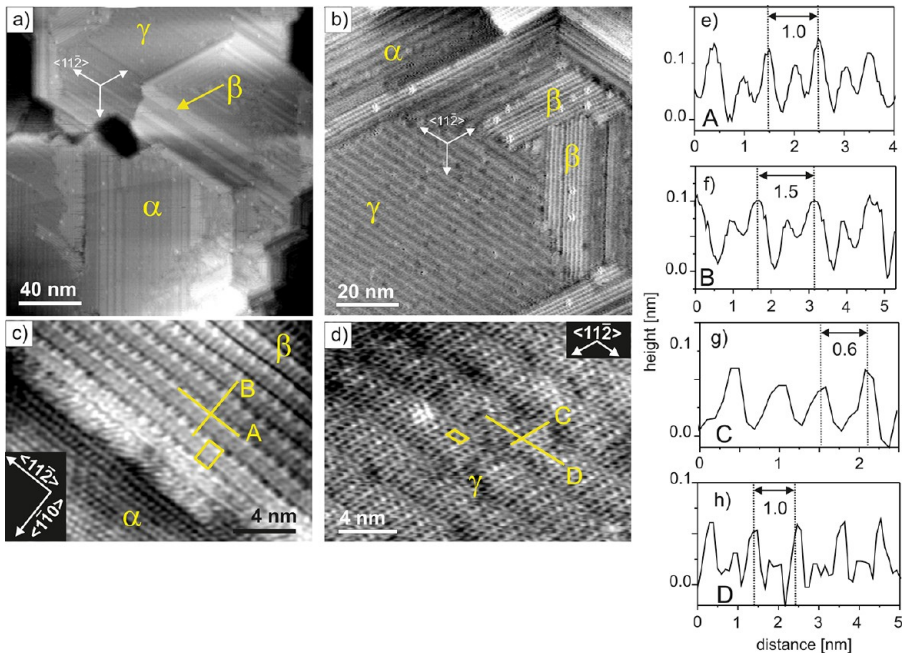

Figure 2. STM data for BP4Se SAMs on Au(111) prepared in 0.1 mM ethanolic solution at 333 K. (a–d) STM images taken with different resolutions. In parts e and f, height profiles A and B are taken along the lines depicted in part c. In parts g and h, heights profiles C and D are taken along the lines depicted in part d. In parts a–d, the α, β, and γ symbols mark different phases (see text for details). In part c, the rectangular box marks the commensurate rectangular $5 \times 2\sqrt{3}$ unit cell of the β-phase with dimensions marked in the height profiles presented in parts e and f, respectively. In part d the oblique box marks the incommensurate oblique $2\sqrt{3} \times 1.2\sqrt{3}$ unit cell of the γ-phase with dimensions marked in the height profiles presented in parts g and h, respectively.

presented in Figure 1c for the α-phase and Figure 1d for the β-phase. Cross section B taken in Figure 1c and presented in Figure 1f indicates that the distance between molecules is well-defined along one of the $\langle 11\bar{2} \rangle$ substrate directions and amounts to ca. 0.5 nm (the average taken from five images give 0.52 ± 0.04 nm) with additional intensity modulation at every second row of molecules. In contrast, cross section A taken in Figure 1c along another equivalent $\langle 11\bar{2} \rangle$ substrate direction (i.e., at the angle of 120° with respect to the direction along cross section B) shows irregular distances between molecules (between ca. 0.5 and 0.8 nm; see Figure 1e) which coincidence with the irregular contrast variation in Figure 1c. The average distance between the molecules along this direction amounts to ca. 0.64 ± 0.04 nm (averaged from five different cross sections). High-resolution data presented in Figure 1d show that the β-phase forms a rectangular structure. The unit cell dimensions of this structure could be determined by the cross sections C and D (see Figure 1g and h) and correspond to about 1.0 nm along one of the $\langle 11\bar{2} \rangle$ substrate directions and 1.5 nm along one of the perpendicular $\langle 1\bar{1}0 \rangle$ directions, respectively.

Data obtained for the BP4Se/Au(111) system are presented in Figure 2. Similarly as for the BP2Se/Au(111) system, large scale data shown in Figure 2a indicate kink formation at step edges and areas corresponding to different STM contrast variation. In this case, however, not two but three different types of contrast patterns could be identified, which are labeled in Figure 2a as α, β, and γ. Higher resolution data presented in Figure 2b clearly show that these three types of contrast patterns correspond to three different structural phases. High resolution data presented in Figure 2c show details of two phases. Cross sections A and B taken in Figure 2c and presented in Figure 2e and f, respectively, clearly indicate that the respective phase structure is identical with the one of the β-phase identified above for BP2Se/Au(111). A similar analysis of the other region visible in Figure 2c (data not shown) revealed that this type of structure is identical with the α-phase identified above for BP2Se/Au(111). High resolution data in Figure 2d enabled identification of a third phase, denoted as the γ-phase, which was not observed for BP2Se/Au(111) and consisted of molecular rows running along one of the $\langle 11\bar{2} \rangle$ substrate directions with alternating contrast of every second row of molecules. The cross section D taken across these molecular rows exhibits intermolecular distances of about 0.5 nm with characteristic contrast variation of every second row of molecules (see Figure 2h), similarly as is observed in the α-phase. This row structure is intersected by regularly spaced contrast lines running along another equivalent $\langle 11\bar{2} \rangle$ substrate direction at the angle of 120°. Cross section C taken in Figure 2d along one of these molecular rows shows a well-defined intermolecular distance of about 0.6 nm (see Figure 2g), in contrast to the irregular distance variation observed in the α-phase along the same substrate direction. This rather regular structure of characteristic contrast variation lines along one of the $\langle 11\bar{2} \rangle$ substrate directions could, at first sight, indicate that the γ-phase consists of molecules arranged in elongated unit cells with the long side determined by the distance between the contrast variation lines. However, a more detailed analysis of the data in Figure 3a (for better contrast, the error signal image is shown) indicates that the observed contrast variation lines (marked in yellow) are in fact regularly spaced translational domain boundaries which separate narrow domain stripes of about 3.5–3.6 nm. These domains are shifted parallel to the direction of the domain boundaries, which in turn run along one of $\langle 11\bar{2} \rangle$ substrate directions, by a small fraction of the total unit cell length (1.0 nm, as marked in the image). As pointed out by the net of white lines in Figure 3a, which mark every

dx.doi.org/10.1021/jp3051998 | J. Phys. Chem. C XXXX, XXX, XXX–XXX

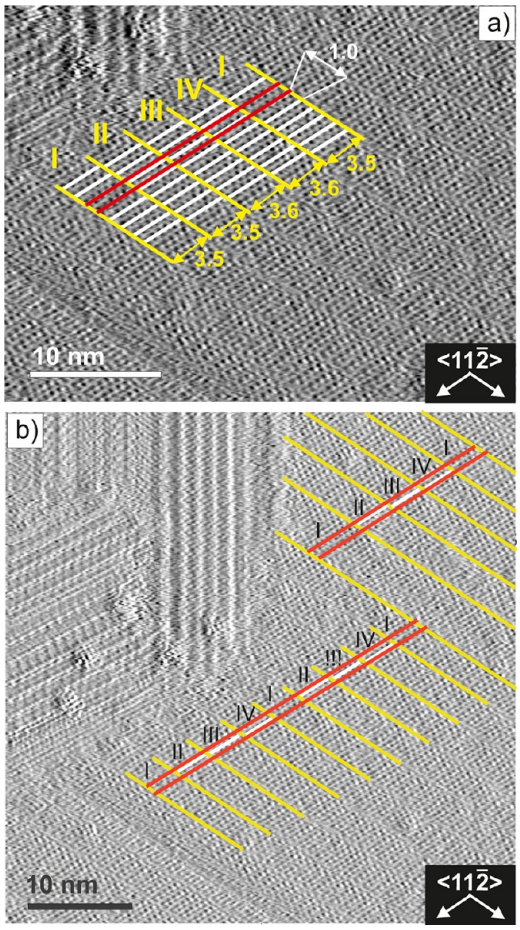

Figure 3. STM data (error signal) for BP4Se SAMs on Au(111) prepared in 0.1 mM ethanolic solution at 333 K. In parts a and b, yellow lines in the γ-phase mark the very regular boundaries of the translational domains with their separation distances of ca. 3.5−3.6 nm depicted in part a and measured along one of the $\langle 11\bar{2}\rangle$ directions. To enable tracking the relative shift of the γ-phase structure between subsequent translational domains in parts a and b, short white lines mark every second molecular row with a separation distance of 1.0 nm (indicated in white) measured along one of the $\langle 11\bar{2}\rangle$ directions. Red lines in parts a and b are shown to track the effect of the periodic cancellation of the relative translational shift after every fourth domain boundary (numbered I−IV; see text for details).

second molecular row in the γ-phase, one can observe that neighboring translational domains numbered I to IV exhibit a systematic shift in the same direction. Interestingly, after crossing four such translational domain boundaries, the structure is back in phase with the domain from which counting was started (assigned by number I). This effect is indicated by two parallel red lines in Figure 3a. Figure 3b shows a larger area scan (error signal image) taken at the same location as data in Figure 3a. Here it can be seen that the effect of periodic cancellation of the translation after every fourth domain boundary is of general character inside any given rotational γ-phase domain.

Data shown in Figure 4 summarize results obtained for the BP6Se/Au(111) system. Similarly as for the two other even-numbered BPnSe/Au(111) SAMs, also in this case, large scale data reveal kink formation at step edges and areas exhibiting different STM contrast (Figure 4a). For BP6Se/Au(111), as in the case of the BP2Se/Au(111) system, only two phases assigned as α and β were observed, which are identified in Figure 4a and b. High resolution data for the α-phase region (Figure 4c) exhibit exactly the same structure as reported above for BP2Se/Au(111) and BP4Se/Au(111). High-resolution data obtained for the β-phase are shown in Figure 4d. The cross sections A and B taken in this image are shown in Figure 4e and f, respectively. The distances which define the dimensions of the β-phase unit cell along one of $\langle 11\bar{2}\rangle$ and $\langle 1\bar{1}0\rangle$ substrate directions are ca. 1.0 and 1.5 nm, respectively. Thus, the β-phase for BP6Se/Au(111) is identical with that identified above for BP2Se/Au(111) and BP4Se/Au(111).

Odd-Numbered BPnSe/Au(111) SAMs (n = 3, 5). Figure 5 summarizes data obtained for BP3Se/Au(111) SAMs. Large scale images (Figure 5a) show similar kinks at step edges as reported above for even-numbered members of the BPnSe/Au(111) series. In this case, however, no regions corresponding to different contrast could be observed. Higher resolution data shown in Figure 5b show different rotational domains of the same structure which are characterized by molecular rows running along one of the $\langle 11\bar{2}\rangle$ substrate directions with alternating contrast of every second row of molecules. The data presented in Figure 5c show additional stripes of contrast modulation within each rotational domain. However, as documented by the cross sections A and B taken in Figure 5d along two of the $\langle 11\bar{2}\rangle$ substrate directions and presented in Figure 5e and f, respectively, these contrast modulation stripes have no influence on the measured intermolecular distances, which are constant and amount to 0.5 nm. The orientation of these stripes is quite regular and ca. 15° off from the closest high symmetry substrate direction, which is one of the $\langle 11\bar{2}\rangle$ directions.

Data obtained for BP5Se/Au(111) are show in Figure 6. Similarly as for BP3Se/Au(111), also in this case a single phase was observed with kink formation at the step edges (Figure 6a). As documented by the high resolution data in Figure 6b and c and the corresponding cross sections presented in Figure 6d and e, this phase is identical with the one observed for the BP3Se/Au(111) system considering both the characteristic stripes of contrast variation within the rotational domains (Figure 6b) and the distances between molecules.

IV. DISCUSSION

Our experiments show clear and systematic differences in the structure of BPnSe/Au(111) SAMs with odd and even numbers of n prepared from solutions at elevated temperature (333 K). However, before a detailed discussion of these differences, we would like to briefly comment on a feature which is common to all measured BPnSe/Au(111) samples, i.e. kink formation at step edges. This effect was also reported in our previous investigations of BPnSe/Au(111) SAMs prepared at room temperature and results from partial change of the substrate step orientation from the $\langle 1\bar{1}0\rangle$ directions, which is characteristic for the bare Au(111) substrate, into the $\langle 11\bar{2}\rangle$ directions after SAM formation.[22] Importantly, such reorientation of substrate step edges was not observed for the thiol analogs (BPnS/Au(111)) prepared in solution at room or elevated temperatures[10] and, thus, indicates higher mobility of gold atoms at the top layer of the substrate upon selenol adsorption as compared to the thiol case. It is well-known that increased strength of the chemical bonding between adsorbate and the metal surface may increase mobility of surface metal atoms.[27,28] Considering this general observation, we have speculated in our previous publication that reorientation of step edges observed for BPnSe/Au(111) SAMs and not for their

dx.doi.org/10.1021/jp3051998 | J. Phys. Chem. C XXXX, XXX, XXX−XXX

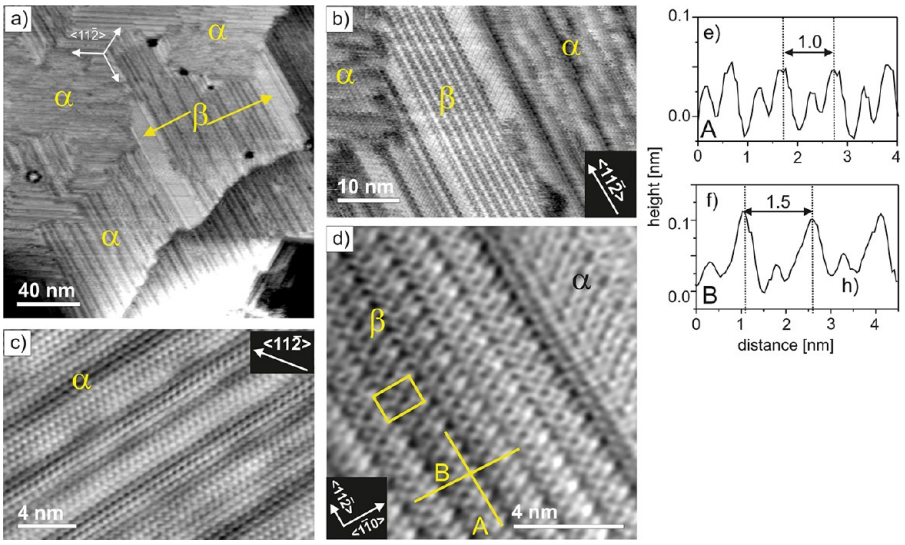

Figure 4. STM data for BP6Se SAMs on Au(111) prepared in 0.1 mM ethanolic solution at 333 K. (a–d) STM images taken with different resolutions. In parts e and f, height profiles A and B are taken along the lines depicted in part d. In parts a–d, the α and β symbols mark different phases (see text for details). In part d, the rectangular box marks the commensurate rectangular $5 \times 2\sqrt{3}$ unit cell of β-phase with dimensions marked in the height profiles presented in parts e and f, respectively.

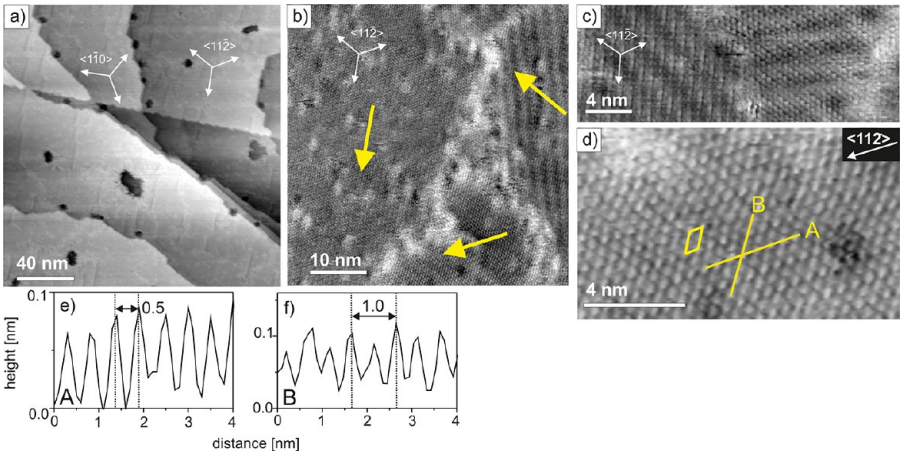

Figure 5. STM data for BP3Se SAMs on Au(111) prepared in 0.1 mM ethanolic solution at 333 K. (a–d) STM images taken with different resolutions. In parts e and f, height profiles A and B are taken along the lines depicted in part d. In part b, yellow arrows mark three different rotational domains following the $\langle 11\bar{2} \rangle$ directions of the substrate. In part d the oblique box marks the commensurate oblique $(2\sqrt{3}\times\sqrt{3})$R30° structure, the dimensions of which are marked in the height profiles presented in parts e and f, respectively.

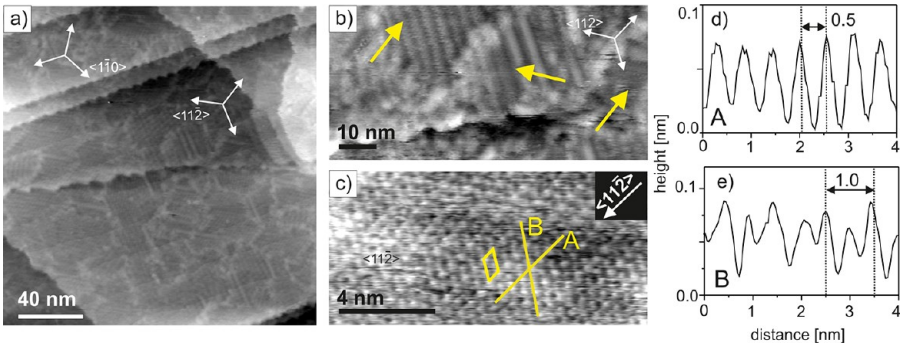

Figure 6. STM data for BP5Se SAMs on Au(111) prepared in 0.1 mM ethanolic solution at 333 K. (a–c) STM images taken with different resolutions. In parts d and e, height profiles A and B are taken along the lines depicted in part c. In part b yellow arrows mark different rotational domains following the $\langle 11\bar{2} \rangle$ directions of the substrate. In part c the oblique box marks the commensurate oblique $(2\sqrt{3}\times\sqrt{3})$R30° structure, the dimensions of which are marked in the height profiles presented in parts d and e, respectively.

dx.doi.org/10.1021/jp3051998 | J. Phys. Chem. C XXXX, XXX, XXX–XXX

thiol analogs indicates higher strength of the Se−Au bonding as compared to the S−Au bond(ing).[22] Importantly, this initial prediction has been fully confirmed by our recent exchange experiments[18] and ion desorption data[25] demonstrating the higher strength of the Se−Au bonds as compared to S−Au in these SAMs.

Turning back to structural differences between odd- and even-numbered BPnSe/Au(111) SAMs prepared at elevated temperatures, we start with a structure common to all even-numbered BPnSe/Au(111) SAMs. As documented by the data in Figures 1, 2, and 4, this is the α-phase, the structure of which is schematically presented in Figure 7. This structure is formed by evenly separated rows of molecules running along one of the $\langle 11\bar{2}\rangle$ substrate directions with characteristic contrast variation of every second row. This contrast variation is typically ascribed to a herringbone arrangement of the biphenyl moieties, as it is found in the solid state structure of biphenyl[29] and is also assumed for most aromatic SAMs.[10,12,21,22,30−34] Interestingly, despite the regular separation between these molecular rows, which allows us to define the respective unit cell vector, the intermolecular distances along these molecular rows are irregular, so that a respective lattice vector cannot be defined. Considering the average distances between the molecules in this structure, the area per molecule is in the range 0.260−0.275 nm^2/molecule. The same structure, having well-defined periodicity only in 1D, was reported previously by us for even-numbered BPnSe/Au(111) prepared at room temperature.[22] However, in contrast to our previous experiments, after preparation at an elevated temperature of 333 K, this 1D ordered structure coexists with one or two other phases which are ordered in 2D. The first 2D ordered structure, assigned as the β-phase, was observed for all even-numbered BPnSe/Au(111) SAMs after deposition at elevated temperature. This structure can be described, as schematically presented in Figure 7, by a commensurate rectangular $5 \times 2\sqrt{3}$ lattice with four molecules per unit cell. The area per molecule in the β-phase structure is about 0.375 nm^2/molecule, which means a 36−44% lower packing density as compared to the α-phase. The second 2D ordered phase, the γ-phase, was observed exclusively for the BP4Se/Au(111) system. Similarly to the α-phase, this structure is formed by evenly separated rows of molecules running along one of the $\langle 11\bar{2}\rangle$ substrate directions. However, in contrast to the α-phase, the distance between molecules along these rows is constant. Thus, an oblique unit cell can be defined in this case as schematically presented in Figure 7. This structure is, however, incommensurate with the substrate along the direction of the molecular rows due to an increased molecular separation of ca. 0.6 nm instead of 0.5 nm. It thus needs to be described by an oblique $2\sqrt{3} \times 1.2\sqrt{3}$ lattice with two molecules per unit cell and the area per molecule of about 0.26 nm^2/molecule, which is similar as for the α-phase. This significant misfit of about 20% between the Au(111) substrate lattice and the γ-phase along one of the $\langle 11\bar{2}\rangle$ substrate directions must generate significant stress. This stress is apparently released by a dense network of translational domain boundaries crossing this structure perpendicular to the misfit direction, i.e. along one of the $\langle 1\bar{1}0\rangle$ directions. Interestingly, the pattern formed by the translational domain boundary is extremely regular regarding both their separation and translation sequence. The distance between these translational domain boundaries typically amounts to 3.5 nm, i.e. the distance which is commensurate with the Au(111) substrate lattice along the $\langle 11\bar{2}\rangle$ directions. Since the system is in phase again after four transitions, the shift in between each translational phase is $^1/_4$ of the b vector of the unit cell, i.e. about 0.25 nm.

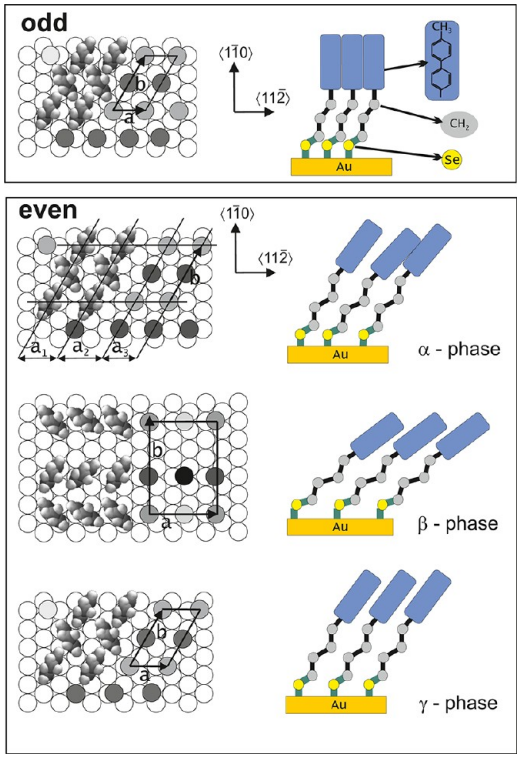

Figure 7. Schematic illustration of the different structures observed at elevated deposition temperature (333 K) for BPnSe SAMs on Au(111) with n = odd (upper panel) and n = even (lower panel). Figures in the right and left columns show schematically the top view and the side view of the structures, respectively. For all structures, herringbone arrangement of phenyl rings was assumed. Open circles in the top view correspond to gold atoms at the Au(111) surface; light and dark gray filled circles correspond to Se atoms with the exact adsorption sites taken to be arbitrary. In the upper panel (n = odd), the commensurate oblique $(2\sqrt{3}\times\sqrt{3})$R30° unit cell is marked by the a and b basis vectors (~0.216 nm^2/molecule). In lower panel (n = even), three different phases are shown with (1) α-phase, for which only the b basis vector is defined whereas the distance a is irregular (shown by different values of a: $a_1 \approx 0.63$ nm, $a_2 \approx 0.73$ nm, and $a_3 \approx 0.53$ nm, ~0.260−0.275 nm^2/molecule); (2) commensurate β-phase described by a rectangular $5 \times 2\sqrt{3}$ unit cell (~0.375 nm^2/molecule); and (3) incommensurate (in a vector direction) γ-phase described by the oblique $2\sqrt{3} \times 1.2\sqrt{3}$ lattice (~0.26 nm^2/molecule).

In summary of this part we would like to underline that the formation of even-numbered BPnSe/Au(111) SAMs at higher temperatures fundamentally changes the way the molecules are arranged on the surface. Whereas the room temperature α-phase structure is ordered only along one surface direction, the β-phase and γ-phase show ordering along two surface directions and thus form fully ordered 2D structures.

Considering now results obtained for odd-numbered BPnSe/Au(111), we point out that for both BP3Se/Au(111) and BP5Se/Au(111) only one common structure was observed. This structure consists of evenly separated rows of molecules along one of the $\langle 11\bar{2}\rangle$ directions exhibiting alternating contrast variation every second row, which presumably can be ascribed to a herringbone arrangement of the biphenyl moieties, similarly as for the α and γ phases in even BPnSe/Au(111)

dx.doi.org/10.1021/jp3051998 | J. Phys. Chem. C XXXX, XXX, XXX−XXX

SAMs. However, in contrast to the α and γ phases, in this case the separation between molecules along these rows is constant and commensurate (or close to commensurate—see text below) with the Au(111) substrate lattice. As schematically shown in Figure 7, this structure could be described by an oblique $(2\sqrt{3}\times\sqrt{3})$R30° lattice with two molecules per unit cell and a packing density of about 0.216 nm^2/molecule. This structure is the same as observed previously for these SAMs prepared at room temperature.[22] Similarly as for the room temperature preparation,[22] also in this case, characteristic stripes with contrast variation are observed which run in a direction off-axis from the high symmetry substrate directions. Importantly, the periodicity of the $(2\sqrt{3}\times\sqrt{3})$R30° lattice as observed by STM is not affected by these additional contrast variations. Following the argumentation proposed in our previous works,[13,22] we believe that this effect results from domain boundaries (solitons) at the molecule−substrate interface and thus indicates that the $(2\sqrt{3}\times\sqrt{3})$R30° lattice can be considered only as an approximation of a not fully commensurate molecular lattice formed by the BP3Se and BP5Se adsorbates.

Taking into consideration all results of the present studies, a clear odd−even effect in polymorphism of BPnSe/Au(111) SAMs is observed with even-numbered systems exhibiting two or three different phases, while the odd-numbered systems are characterized by a single phase. We note here that such polymorphism of BPnSe/Au(111) SAMs was not observed for samples prepared at room temperature, and only preparation at elevated temperature revealed the new phases of the even-numbered members of this homologous series. This indicates lower thermal stability of room temperature phase for even-numbered BPnSe/Au(111) SAMs, which upon annealing start to coexist with other phases. To address the possible mechanism responsible for this odd−even effect in BPnSe/Au(111) SAMs stability, we point out that similar odd−even effects in polymorphism were observed previously by us for thiol analogs of these SAMs, i.e. for the BPnS/Au(111) series.[35−37] Importantly, this odd−even polymorphism of BPnSe/Au(111) and BPnS/Au(111) SAMs is following other related similarities between these systems, i.e. a very similar odd−even effect in their structure[22,23] (when prepared at room temperature) as well as odd−even effects regarding their stability toward exchange by aliphatic SAMs (alkanethiols and alkaneselenols, respectively)[18] and ion-induced desorption.[16,25] Considering all these similarities, we believe that the simple phenomenological model proposed by us previously[36] to explain different stabilities in the BPnS/Au(111) systems could also be applied for BPnSe/Au(111) SAMs. Following our previous argumentation, the difference in stability of odd- and even-numbered BPnSe/Au(111) SAMs could be explained by the way in which factors, such as coverage, intermolecular interactions, and bonding configuration at the molecule−substrate interface (defined by the C−Se−Au angle), work together to determine the energy balance of a SAM (see Figure 11 in ref 36). In this model, the bonding configuration at the molecule−substrate interface contributes significantly to the energetics of the SAM, and its stability depends on whether this factor can be optimized *along with* the other two factors (cooperatively) or *at the expense of* these factors (competitively). The cooperative way leading to a stable system is realized in odd-numbered BPnSe/Au(111) SAMs in which high coverage structure and optimized intermolecular interactions can be achieved simultaneously with the optimized C−Se−Au bonding configuration defined by the C−Se−Au bond angle and the Se adsorption sites on the Au(111) substrate. The opposite situation applies for the even-numbered BPnSe/Au(111) SAMs where competition between optimization of the C−Se−Au bonding configuration and the other two factors leads to the formation of structures with lower stability.

Present experiments indicate also clear differences between the stability of BPnSe/Au(111) SAMs and their thiols analogs, i.e. BPnS/Au(111). An interesting difference regards the formation of the β-phase, which has a significantly lower packing density (36−44%) than the room temperature α-phase, which in turn has very similar packing density for BPnSe/Au(111) and BPnS/Au(111) SAMs. Since under the present experimental conditions a full transition into the β-structure was not achieved, we could not probe the stability of this new phase. Importantly, preparing BPnS/Au(111) SAMs at a solution temperature of 333 K did not result in any phases with a lower packing density.[10] New phases for even-numbered BPnS/Au(111) SAMs were only observed when samples prepared at room temperature were annealed at much higher temperatures (starting from 373 K).[35−37] This observation could lead to the conclusion that the BPnSe molecules are much more weakly bound to the Au(111) substrate than their thiol analogs. This, however, contradicts our present observation regarding the reorientation of the substrate steps as well as previous exchange[18] and desorption experiments[25] which clearly indicated higher stability of the Au−Se bonding as compared to the Au−S in these SAMs. However, these experiments indicated that the higher strength of the Au−Se bonding results in weakening of the $Au_{surface}$−Au_{bulk} bonds (substrate steps reorientation in the present experiments) as well as the Se−C bonds (desorption experiments[25]). Thus, reorganization of the BPnSe/Au(111) structure at higher incubation temperature and lack of such an effect for BPnS/Au(111) results from complex changes at the SAM−substrate interface induced by the S → Se substitution. These changes are not only limited to the Au−S(Se) bond stability but also to the related mobility of the surface gold atoms and stability of the S(Se)−C bond. As is documented by the present experiments, all these processes have a profound impact on the molecule−substrate interface and, thus, on the resulting film structure.

Since the observed transition to the β- and γ-phase is only partial, it remains impossible at the moment to decide whether formation of these phases is thermodynamically or kinetically controlled. It should be noted, however, that for the thiol analogs (BPS/Au(111)) similar transitions to lower density structures such as the β-phase[36] led to much more stable structures than the respective room temperature phase. Thus, lowering the packing density (to some extend) in the SAMs investigated here does not ultimately mean a reduction of the film stability. As discussed in our former paper,[36] surface stress arising from the misfit between the lattices of aromatic SAMs and the Au(111) substrate[13] is an important contribution to the overall film stability and may be compensated by lowering the film density.

It seems that surface stress reduction could also be an origin for γ-phase formation. In this case, the surface coverage remains virtually unchanged, since the BPnSe lattice on the Au(111) surface simply undergoes a transition along the $\langle 11\bar{2}\rangle$ surface direction. As a result, the disorder along this direction of the α-phase is transferred into the ordered but incommensurate structure of the γ-phase. The surface stress induced by the

dx.doi.org/10.1021/jp3051998 | J. Phys. Chem. C XXXX, XXX, XXX−XXX

structural misfit in the γ-phase is reduced in a very specific way by the formation of an extremely regular network of translation domains. In addition, the distance between the boundaries of these translation domains is commensurate with the Au(111) substrate lattice. Such an "elegant" solution for surface stress-relaxation was observed, under our experimental conditions, exclusively for the BP4Se/Au(111) system. Since the intermolecular interactions in BPnSe SAMs are mainly governed by the interactions between phenyl rings (π stacking), observation of the γ-phase for only one certain length of even-numbered alkyl spacer indicates a very high sensitivity of the detailed course of the phase transition depending on the interplay of the factors governing the energetics and kinetics of these SAMs.

V. SUMMARY

In summary, the data obtained from BPnSe/Au(111) SAMs prepared at elevated solution temperatures revealed several important features related to the S → Se substitution in SAMs. First we observed an odd−even effect in the polymorphism of BPnSe/Au(111) SAMs that is similar to the one for their thiol analogs. This information is important since it allows us to propose a model in which the bonding configuration at the molecule−substrate interface contributes dominantly to the energetics of the SAM. In this model, the stability of a certain SAM structure depends on whether the bonding configuration at the molecule−substrate interface can be optimized *along with* (cooperatively) or *at the expense of* (competitively) two other factors (surface coverage and intermolecular interactions), resulting in a stable or unstable film, respectively. Furthermore, the appearance of new phases in the BPnSe/Au(111) SAMs at much lower temperatures than for BPnS/Au(111) indicates that S → Se substitution has a complex influence on the SAM−substrate interface. This influence is not only limited to the increased strength of the Au−Se bond as compared to Au−S bond but also to the reduced, as a consequence of this increase, strength of the $Au_{surface}$−Au_{bulk} and Se−C bonding.

AUTHOR INFORMATION

Corresponding Author

*E-mail: piotr.cyganik@.uj.edu.pl.

Notes

The authors declare no competing financial interest.

ACKNOWLEDGMENTS

The authors would like to thank Professor Marek Szymonski for providing the access to the STM microscope at the Department of Physics of Nanostructures and Nanotechnology at the Jagiellonian University. The work was supported by the Polish Ministry of Science and Higher Education (0061/B/H03/2008/34). P.C. greatly acknowledges a *Homing* fellowship by the Foundation for Polish Science.

REFERENCES

(1) Love, J. C.; Estroff, L. A.; Kriebel, J. K.; Nuzzo, R. G.; Whitesides, G. M. *Chem. Rev.* **2005**, *105*, 1103−1170.
(2) Vericat, C.; Vela, M. E.; Benitez, G.; Carro, P.; Salvarezza, R. C. *Chem. Soc. Rev.* **2010**, *39*, 1805−1834.
(3) Maksymovych, P.; Voznyy, O.; Dougherty, D. B.; Sorescu, D. C.; Yates, J. T. *Prog. Surf. Sci.* **2010**, *85*, 206−240.
(4) Song, H.; Reed, M. A.; Lee, T. *Adv. Mater.* **2011**, *23*, 1583−1608.
(5) McCreery, R. L.; Bergren, A. J. *Adv. Mater.* **2009**, *21*, 4303−4322.
(6) Zharnikov, M.; Frey, S.; Rong, H. T.; Yang, Y. J.; Heister, K.; Buck, M.; Grunze, M. *Phys. Chem. Chem. Phys.* **2000**, *2*, 3359−3362.
(7) Rong, H. T.; Frey, S.; Yang, Y. J.; Zharnikov, M.; Buck, M.; Wühn, M.; Wöll, C.; Helmchen, G. *Langmuir* **2001**, *17*, 1582−1593.
(8) Heister, K.; Rong, H. T.; Buck, M.; Zharnikov, M.; Grunze, M.; Johansson, L. S. O. *J. Phys. Chem. B* **2001**, *105*, 6888−6894.
(9) Azzam, W.; Cyganik, P.; Witte, G.; Buck, M.; Wöll, C. *Langmuir* **2003**, *19*, 8262−8270.
(10) Cyganik, P.; Buck, M.; Azzam, W.; Wöll, C. *J. Phys. Chem. B* **2004**, *108*, 4989−4969.
(11) Azzam, W.; Fuxen, C.; Birkner, A.; Rong, H. T.; Buck, M.; Wöll, C. *Langmuir* **2003**, *19*, 4958−4968.
(12) Käfer, D.; Witte, G.; Cyganik, P.; Terfort, A.; Wöll, C. *J. Am. Chem. Soc.* **2006**, *128*, 1723−1732.
(13) Cyganik, P.; Buck, M.; Wilton-Ely, J. D.; Wöll, C. *J. Phys. Chem. B* **2005**, *109*, 10902−10908.
(14) Long, Y. T.; Rong, H. T.; Buck, M.; Grunze, M. *J. Electroanal. Chem.* **2002**, *524*, 62−67.
(15) Thom, I.; Buck, M. *Surf. Sci.* **2005**, *581*, 33−46.
(16) Vervaecke, F.; Wyczawska, S.; Cyganik, P.; Bastiaansen, J.; Postawa, Z.; Silverans, R. E.; Vandeweert, E.; Lievens, P. *ChemPhysChem* **2011**, *12*, 140−144.
(17) Felgenhauer, T.; Rong, H. T.; Buck, M. *J. Electroanal. Chem.* **2003**, *550*, 309−319.
(18) Szelagowska-Kunstman, K.; Cyganik, P.; Schüpbach, B.; Terfort, A. *Phys. Chem. Chem. Phys.* **2010**, *12*, 4400−4406.
(19) Frey, S.; Rong, H. T.; Heister, K.; Yang, Y. J.; Buck, M.; Zharnikov, M. *Langmuir* **2002**, *18*, 3142−3150.
(20) Shaporenko, A.; Cyganik, P.; Buck, M.; Terfort, A.; Zharnikov, M. *J. Phys. Chem. B* **2005**, *109*, 13630−13638.
(21) Bashir, A.; Käfer, D.; Müller, J.; Wöll, C.; Terfort, A.; Witte, G. *Angew. Chem., Int. Ed.* **2008**, *47*, 5250−5253.
(22) Cyganik, P.; Szelagowska-Kunstman, K.; Terfort, A.; Zharnikov, M. *J. Phys. Chem. C* **2008**, *112*, 15466−15473.
(23) Weidner, T.; Shaporenko, A.; Müller, J.; Schmid, T.; Cyganik, P.; Terfort, A.; Zharnikov, M. *J. Phys. Chem. C* **2008**, *112*, 12495−12506.
(24) Shaporenko, A.; Müller, J.; Weidner, T.; Terfort, A.; Zharnikov, M. *J. Am. Chem. Soc.* **2007**, *129*, 2232−2233.
(25) Wyczawska, S.; Cyganik, P.; Terfort, A.; Lievens, P. *ChemPhysChem* **2011**, *12*, 2554−2557.
(26) Müller, J.; Terfort, A. *Inorg. Chim. Acta* **2006**, *359*, 4821−4827.
(27) Sette, F.; Hashizume, T.; Comin, F.; MacDowell, A. A.; Citrin, P. H. *Phys. Rev. Lett.* **1988**, *61*, 1384−1387.
(28) Trevor, D. J.; Chidsey, C. E. D.; Loiacono, D. N. *Phys. Rev. Lett.* **1989**, *62*, 926−932.
(29) Trotter, J. *Acta Crystallogr.* **1961**, *14*, 1135−1140.
(30) Käfer, D.; Bashir, A.; Witte, G. *J. Phys. Chem. C* **2007**, *111*, 10546−10551.
(31) Kang, J. F.; Ulman, A.; Liao, S.; Jordan, R.; Yang, G. H.; Liu, G. Y. *Langmuir* **2001**, *17*, 95−106.
(32) Yang, G. H.; Liu, G. Y. *J. Phys. Chem. B* **2003**, *107*, 8746−8759.
(33) Chesneau, F.; Schüpbach, B.; Szelagowska-Kunstman, K.; Ballav, N.; Cyganik, P.; Terfort, A.; Zharnikov, M. *Phys. Chem. Chem. Phys.* **2010**, *12*, 12123−12137.
(34) Azzam, W.; Bashir, A.; Terfort, A.; Strunskus, T.; Wöll, C. *Langmuir* **2006**, *22*, 3647−3655.
(35) Cyganik, P.; Buck, M. *J. Am. Chem. Soc.* **2004**, *126*, 5960−5961.
(36) Cyganik, P.; Buck, M.; Strunskus, T.; Shaporenko, A.; Wilton-Ely, J. D. E. T.; Zharnikov, M.; Wöll, C. *J. Am. Chem. Soc.* **2006**, *128*, 13868−13878.
(37) Cyganik, P.; Buck, M.; Strunskus, T.; Shaporenko, A.; Witte, G.; Zharnikov, M.; Wöll, C. *J. Phys. Chem. C* **2007**, *111*, 16909−16911.